Chinese Journal of Electronics
vol. 33, no. 1, pp. 195–203, January 2024
https://doi.org/10.23919/cje.2022.00.161

RESEARCH ARTICLE

Visible Light Indoor Positioning System Based on Pisarenko Harmonic Decomposition and Neural Network

Li ZHAO, Yi REN, Qi WANG, Lange DENG, and Feng ZHANG

School of Electronic Information Engineering, Xi'an Technological University, Xi'an 710021, China

Corresponding author: Li ZHAO, Email: pilly_lily@126.com
Manuscript Received June 12, 2022; Accepted July 30, 2022

Abstract — Visible-light indoor positioning is a new generation of positioning technology that can be integrated into smart lighting and optical communications. The current received signal strength (RSS)-based visible-light positioning systems struggle to overcome the interferences of background and indoor-reflected noise. Meanwhile, when ensuring the lighting, it is impossible to use the superposition of each light source to accurately distinguish light source information; furthermore, it is difficult to achieve accurate positioning in complex indoor environments. This study proposes an indoor positioning method based on a combination of power spectral density detection and a neural network. The system integrates the mechanism for visible-light radiation detection with RSS theory, to build a back propagation neural network model fitting for multiple reflection channels. Different frequency signals are loaded to different light sources at the beacon end, and the characteristic frequency and power vectors are obtained at the location end using the Pisarenko harmonic decomposition method. Then, a complete fingerprint database is established to train the neural network model and conduct location tests. Finally, the location effectiveness of the proposed algorithm is verified via actual positioning experiments. The simulation results show that, when four groups of sinusoidal waves with different frequencies are superimposed with white noise, the maximum frequency error is 0.104 Hz and the maximum power error is 0.0362 W. For the measured positioning stage, a 0.8 m × 0.8 m × 0.8 m solid wood stereoscopic positioning model is constructed, and the average error is 4.28 cm. This study provides an effective method for separating multi-source signal energies, overcoming background noise, and improving indoor visible-light positioning accuracies.
Keywords — Visible-light communication, Indoor positioning, Frequency estimation, Pisarenko harmonic decomposition, Back propagation neural network.
Citation — Li ZHAO, Yi REN, Qi WANG, *et al.*, "Visible Light Indoor Positioning System Based on Pisarenko Harmonic Decomposition and Neural Network," *Chinese Journal of Electronics*, vol. 33, no. 1, pp. 195–203, 2024. doi: 10.23919/cje.2022.00.161.

I. Introduction

With the gradual maturation of visible-light communication technology and the in-depth study of indoor-positioning-related applications, indoor positioning technology has attracted increasing attention from researchers at home and abroad [1], [2]. The technology combines lighting and communication, and offers rich spectrum resources without electromagnetic interference [3], [4]. It has numerous advantages over traditional radio frequency communications [5], [6]. In recent years, it has become a new research hotspot in the field of wireless technology [7], [8].

The received signal strength (RSS) localization algorithm is based upon the photodetectors and is widely used because it offers a simple theoretical implementation and strong portability [9], [10]. However, when used to ensure lighting, it fails to accurately obtain the attenuation factor of each light-emitting diode (LED) light [11], [12]; hence, it cannot position precisely [13], [14]. To solve these problems, one study [15] adopted centralized single-array light-source illumination, and the receiver effectively solved the problem of light-source discrimination detection by using a four-array symmetrical pho-

Associate Editor: Prof. Xizheng KE, Xi'an University of Technology.

todetectors (PD) layout. However, the centralized single-array illumination has poor illumination uniformity (which leads to problems of communication blind spots), and the positioning error is as large as 12.65 cm. To solve the blind spot problem of single-array communications, reference [16] proposed a code division multiple access (CDMA) RSS triangle positioning method based on diversity reception technology. The method adopted three LEDs and arranged them to control the positioning accuracy to within 10 cm. However, the method required the support of coding technology, which increased the system complexity. Reference [17] proposed an indoor three-dimensional space positioning algorithm based on a mixture of RSS and arrival angle information. The least squares method was used to establish the optimization objective function and derive the least squares estimator. It could control the positioning error to within 8.7 cm; however, it placed strict demands upon time synchronization. In [18], a receiver-signal-strength-aided perspective three-point localization algorithm was proposed. The position of the receiver was estimated using visual and intensity information. The simulation results show that the method could realize a positioning accuracy lower than 10 cm in more than 70% of the indoor area, though the positioning error was large because the directions of the LED and receiver were neglected. The power spectral density (PSD) detection algorithm had a high frequency identification ability. Combined with the nonlinear mapping ability of a neural network, it could effectively separate the attenuation factors of multi-array LED lights in the spatial transmission process and fit the nonlinear mapping relationship between the receiving power and position coordinate [19], to achieve high-precision positioning.

Therefore, on the premise of ensuring lighting, the power discrimination and precise positioning of visible light indoor positioning can be realized at the same time. we propose an indoor-positioning method based on PSD detection and a neural network. It can distinguish and extract the light signals for different frequencies, by loading different frequency signals to different light sources at the beacon end and selecting the appropriate PSD detection method at the position detection end; then, the separate light signals are applied to the neural network to achieve real-time and accurate positioning.

II. Location Algorithm Based on Pisarenko Decomposition and Neural Network

The interference of multiple reflections and background light means that the received power is non-linearly mapped to the position coordinates. It is difficult to overcome the influence of background noise and multiple reflections in the traditional RSS positioning process [20]. Therefore, this study adopts a neural network combined with the RSS positioning principle [21], [22], and it proposes a positioning algorithm based on Pisarenko decomposition and a neural network. The principle is shown in Figure 1. Multiple LED light source signals are modulated using sine waves of different frequencies; then, these are sent to the drive circuit, which drives multiple LED

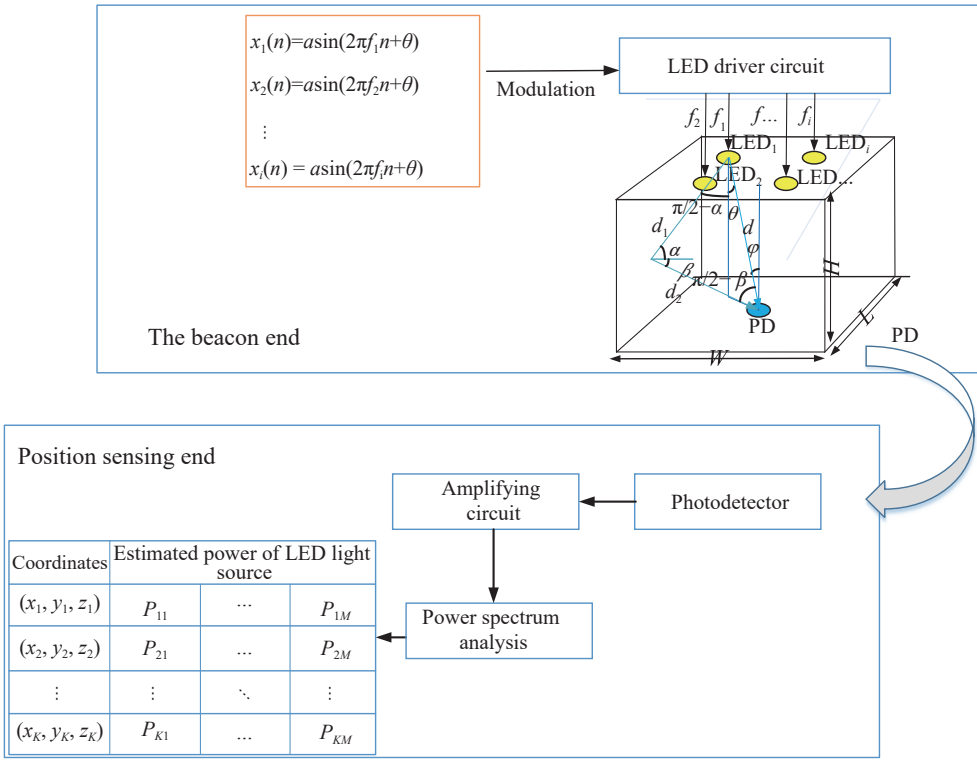

Figure 1 Location algorithm based on Pisarenko decomposition and neural network.

lights to emit multiple light signals with different frequencies. The energy databases of each light source, as established by Pisarenko decomposition, are separated to form the training and test data, Finally, these are inputted to a back-propagation (BP) neural network for training and testing [23], [24].

1. Data separation and database establishment based on Pisarenko decomposition

Assuming that the i-th LED at the transmitter is driven by a sinusoidal signal of frequency f_i, the signal at the transmitter is

$$x_i(n) = A_i \sin(2\pi f_i n)(1 \le i \le M) \tag{1}$$

where A_i is the amplitude of the modulation signal, and f_i is the frequency of the optical power signal generated by the i-th LED light source.

By the linear properties of sine signals, we have that

$$\begin{aligned}&\sin(2\pi f_i n + \varphi) + \sin\left[2\pi f_i (n-2) + \varphi\right] \\ &\quad = 2\cos(2\pi f_i)\sin\left[2\pi f_i (n-1) + \varphi\right]\end{aligned} \tag{2}$$

Substituting (1) into (2), we obtain the difference equation:

$$x(n) - 2\cos(2\pi f_i)x(n-1) + x(n-2) = 0 \tag{3}$$

Z transformation is performed on both sides of (3), which yields

$$\left[1 - 2\cos(2\pi f_i)z^{-1} + z^{-2}\right] X(z) = 0 \tag{4}$$

Thus,

$$1 - 2\cos(2\pi f_i)z^{-1} + z^{-2} = 0 \tag{5}$$

The two results of (5) are

$$z = \cos\omega \pm \mathrm{j}\sin\omega = \mathrm{e}^{\pm \mathrm{j}2\pi f_i} \tag{6}$$

Therefore, the frequency of the sine wave is

$$f_i = \frac{1}{2\pi}\arctan\left[\frac{\mathrm{Im}(z_i)}{\mathrm{Re}(z_i)}\right] \tag{7}$$

When M LED lights are simultaneously driven by different frequency signals, the root can be determined using

$$\prod_{i=1}^{M}(z - z_i)(z - z_i^*) = \sum_{i=0}^{2M} a_i z^{2M-i} = 0 \tag{8}$$

The $a_0 = 1$ coefficients exhibit a symmetry of $a_i = a_{2M-I}\,(I = 0, 1, \ldots, M)$. The difference equation of (8) is

$$x\,(n) + \sum_{i=1}^{2M} a_i x(n-i) = 0 \tag{9}$$

The visible-light signal received by the receiver can be expressed as [25], [26]

$$y(n) = x(n) + e(n) = H(0)A_n(2\pi f_n t) + \sigma^2_{\mathrm{noise}} \tag{10}$$

where $H\,(0)$ is the channel DC gain of the fitted multiple reflection channel [27], [28], and can be expressed as

$$\begin{aligned}H\,(0) =& H_{\mathrm{LOS}}\,(0) + H^1_{\mathrm{NLOS}}\,(0) \\ =& \frac{(m_1+1)A}{2\pi d^2}\cos^{m_1}(\theta)T_S(\varphi)g(\varphi)\cos(\varphi) \\ &+ \frac{(m_1+1)A}{2\pi d_1^2 d_2^2}\cdot dS_f T_S(\varphi)\rho\cos\alpha\cos\beta\cos^{m_1}(\theta)\cos(\varphi)\end{aligned} \tag{11}$$

where $H_{\mathrm{LOS}}(0)$ and $H^1_{\mathrm{NLOS}}(0)$ represent DC gain and primary reflection gain, respectively, and m_1 represents the Lambertian luminescence order at the emitter, θ is the transmission angle relative to the vertical axis of LED, φ is the incident angle relative to the receiving axis, α and β are the incident angle and the outgoing angle of the reflected light signal respectively. D is the distance between the sending and receiving ends, d_1 and d_2 are the distances from the LED to reflection point and reflection point to receiver respectively. ρ is the reflection coefficient, and dS_f is the area element of the reflector. $T_S(\varphi)$ is the optical filter gain, and $g(\varphi)$ is the collector gain [29], [30].

Substituting (12) into (9), we obtain

$$y(n) + \sum_{i=1}^{2M} a_i y(n-i) = e(n) + \sum_{i=1}^{2M} a_i e(n-i) \tag{12}$$

where $y(n)$ denote the observations with noise $e(n)$, $x(n)$ is the original signal without noise. Equation (12) is written in matrix form as

$$Y^{\mathrm{T}}A = E^{\mathrm{T}}A \tag{13}$$

$$\begin{cases} Y = [y(n), y(n-1), \ldots, y(n-2M)]^{\mathrm{T}} \\ A = (1, a_1, \ldots, a_{2M})^{\mathrm{T}} \\ E = [e(n), e(n-1), \ldots, e(n-2M)]^{\mathrm{T}} \end{cases} \tag{14}$$

Multiply both sides of (13) to the left by the vector Y, Taking the mathematical expectation on both sides simultaneously, we obtain

$$R_Y A = \sigma_e^2 A \tag{15}$$

where

$$\begin{aligned}R_Y &= E\left\{yy^{\mathrm{T}}\right\} \\ &= \begin{bmatrix} R_y(0) & R_y(-1) & \ldots & R_y(-2M) \\ R_y(1) & R_y(0) & \ldots & R_y(-2M+1) \\ \vdots & \vdots & \ddots & \vdots \\ R_y(2M) & R_y(2M-1) & \ldots & R_y(0) \end{bmatrix}\end{aligned} \tag{16}$$

R_Y is the auto-correlation matrix of the observation

process $y(n)$, σ_e^2 is the characteristic values λ_I of R_Y. The coefficient vector A of the characteristic polynomial corresponds to the eigenvalue of eigenvector λ_i. The dimension of the noise subspace is 1, which is composed of the feature vector corresponding to the minimum eigenvalue $\lambda_{\min} = \sigma_e^2$. When applying the Pisarenko harmonic decomposition method to a p $(p > 2M)$ dimension auto-correlation matrix R_Y, to avoid multiple eigenvalues and multiple solutions of the coefficient vector A, it is necessary to apply dimension-reduced processing:

$$E\left\{yy^{\mathrm{T}}\right\} = \begin{bmatrix} R_y(0) & R_y(-1) & \dots & R_y(-M) \\ R_y(1) & R_y(0) & \dots & R_y(-M+1) \\ \vdots & \vdots & \ddots & \vdots \\ R_y(M) & R_y(M-1) & \dots & R_y(0) \end{bmatrix} \stackrel{\text{def}}{=} R_Y \tag{17}$$

To solve the coefficient matrix A of the characteristic polynomial in (14), the frequency of each sine signal can be calculated using (7). Because of the statistical independence between signal $x(n)$ and white noise $e(n)$, the auto-correlation matrix of the received signal $y(n)$ can be expressed as (18) via (10).

$$R_y(k) = R_x(k) + R_e(k) = \sum_{i=1}^{M} P_i e_i e_i^{\mathrm{H}} + \sigma_\omega^2 I \tag{18}$$

Here, $e_i = [1, \mathrm{e}^{\mathrm{j}2\pi f_i}, \mathrm{e}^{\mathrm{j}2(2\pi f_i)}, \dots, \mathrm{e}^{\mathrm{j}(M-1)2\pi f_i}]$ $(i = 1, 2, \dots, M)$ denote M linearly independent vectors. And $P_i = |A_i|^2$ is the power of the light signal emitted by the i-th LED light, as detected at the receiving end.

Assuming that the eigenvectors $a_1, a_2, \dots, a_M$ of the signal subspace are normalized, we have that $a_i a_i^{\mathrm{H}} = 1$. Because

$$R_Y a_i = \lambda_i a_i,\ i = 1, 2, \dots, M \tag{19}$$

we multiply both sides of the above formula by a_i^{H} from the left, and get

$$a_i^{\mathrm{H}} R_Y a_i = \lambda_i a_i^{\mathrm{H}} a_i = \lambda_i,\ i = 1, 2, \dots, M \tag{20}$$

We substitute R_Y (see (18)) into the above formula, thus,

$$a_i^{\mathrm{H}} R_Y a_i = a_i^{\mathrm{H}} \left\{ \sum_{k=1}^{M} P_k e_k e_k^{\mathrm{H}} + \sigma_\omega^2 I \right\} a_i = \lambda_i \tag{21}$$

Simplifying this gives us

$$\sum_{k=1}^{M} P_k \left| e_k^{\mathrm{H}} a_i \right|^2 = \lambda_i - \sigma_\omega^2,\ i = 1, 2, \dots, M \tag{22}$$

where $\left|e_k^{\mathrm{H}} a_i\right|^2$ is the square amplitude of the discrete-time Fourier transform for signal subspace eigenvector a_i at frequency f_k. We have that

$$\left|e_k^{\mathrm{H}} a_i\right|^2 = \left|A_i(\mathrm{e}^{\mathrm{j}\omega k})\right|^2 \tag{23}$$

Hence, equation (22) can be written as

$$\sum_{k=1}^{M} P_k \left|A_i(\mathrm{e}^{\mathrm{j}\omega k})\right|^2 = \lambda_i - \sigma_\omega^2,\ i = 1, 2, \dots, M \tag{24}$$

The above equation expresses M linear equations, which have M unknown parameters P and can be written in matrix form as follows:

$$\begin{bmatrix} \left|A_1(\mathrm{e}^{\mathrm{j}\omega 1})\right|^2 & \left|A_1(\mathrm{e}^{\mathrm{j}\omega 2})\right|^2 & \dots & \left|A_1(\mathrm{e}^{\mathrm{j}\omega M})\right|^2 \\ \left|A_2(\mathrm{e}^{\mathrm{j}\omega 1})\right|^2 & \left|A_2(\mathrm{e}^{\mathrm{j}\omega 2})\right|^2 & \dots & \left|A_2(\mathrm{e}^{\mathrm{j}\omega M})\right|^2 \\ \vdots & \vdots & \ddots & \vdots \\ \left|A_M(\mathrm{e}^{\mathrm{j}\omega 1})\right|^2 & \left|A_M(\mathrm{e}^{\mathrm{j}\omega 2})\right|^2 & \dots & \left|A_M(\mathrm{e}^{\mathrm{j}\omega M})\right|^2 \end{bmatrix} \times \begin{bmatrix} P_1 \\ P_2 \\ \vdots \\ P_M \end{bmatrix} = \begin{bmatrix} \lambda_1 - \sigma_\omega^2 \\ \lambda_2 - \sigma_\omega^2 \\ \vdots \\ \lambda_M - \sigma_\omega^2 \end{bmatrix} \tag{25}$$

The power matrix $P = [P_1, P_2, \dots, P_M]$, can be obtained by solving (25). P_i is the power of the i-th LED light detected at the receiver, which is the input power for the input layer of the neural network. The final positioning coordinates can be obtained by repeatedly training and testing the neural network.

2. Position estimation based on BP neural network

As shown in Figure 2, the neural network is a three-layer BP one. The input of the input layer is the power matrix P, which is extracted from the Pisarenko decomposition in (24); the outputs of the output layer are the relative coordinates of the unknown positioning points.

We randomly select Q points in the plane of positioning area $H = 0$ m as the reference point of the fingerprint data sample; the number of training datasets is K, and the sample number of test datasets is L $(L + K = Q)$. The matrix constructed via the PSD estimation of the M LED light sources received by each fingerprint point is the input training set $\boldsymbol{X}^{\mathrm{T}}$:

$$\boldsymbol{X}^{\mathrm{T}} = \begin{pmatrix} X_1 \\ X_2 \\ \vdots \\ X_K \end{pmatrix}^{\mathrm{T}} = \begin{pmatrix} P_{11}, P_{12}, \dots, P_{1M} \\ P_{21}, P_{22}, \dots, P_{2M} \\ \vdots \\ P_{K1}, P_{K2}, \dots, P_{KM} \end{pmatrix}^{\mathrm{T}}_{K \times M} \tag{26}$$

Here, $\boldsymbol{X}_d = (P_{d1}, P_{d2}, \dots, P_{dM})$ $(1 \le d \le K)$ represents the power estimation of M LED light sources received at the d position reference point. P_{dM} represents the optical power value of the M-th LED light source received by the n-th fingerprint at position (x_n, y_n, z_n).

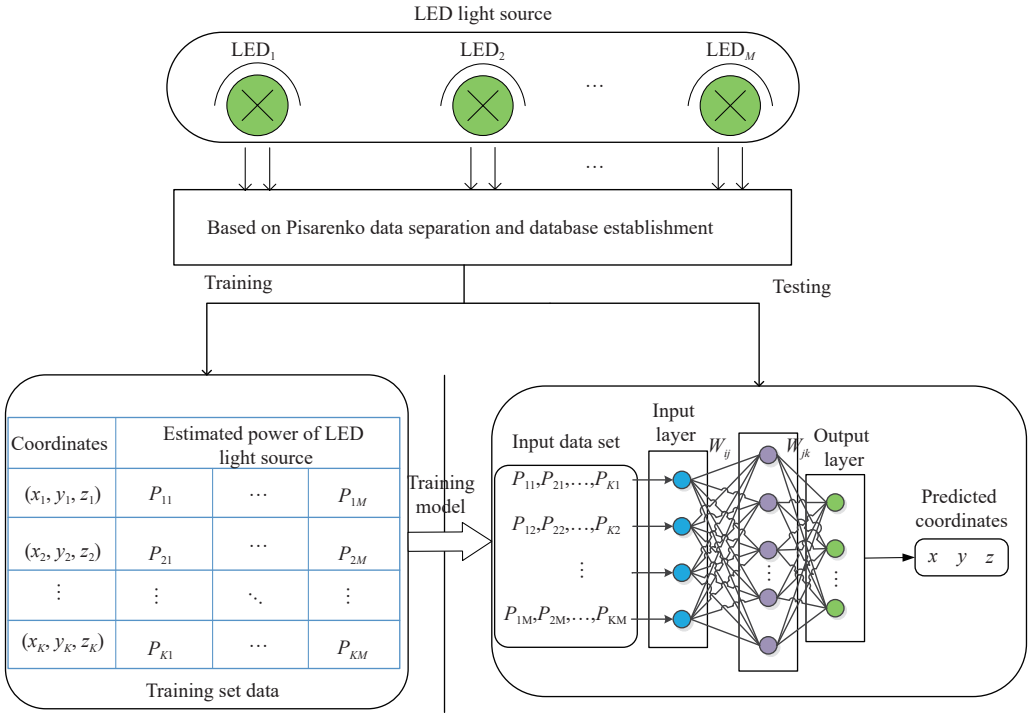

Figure 2 Schematic diagram of neural-network-based visible-light localization.

For each training sample, we calculate the output of each neuron from forward to backward. The excitation function is a unipolar S-type function, expressed as [31]

$$f(x) = \frac{1}{1+\mathrm{e}^{-\beta x}},\ \beta > 0 \tag{27}$$

The output layer weight coefficient is

$$\Delta\theta_k = -\eta\beta O_k(1-O_k)(d_k - O_k) \tag{28}$$

where η is the learning rate. The net input of the k-th node in the output layer is $I_k = \sum_{j=0}^{Q} w_{jk}O_j$. The net output is $O_k = f(I_k)$.

The weight coefficient of the hidden layer is

$$\Delta w_{ij} = \eta\delta_j O_i = \eta\beta O_i O_j(1-O_j)\sum_{k=1}^{L}\delta_k w_{jk} \tag{29}$$

The matrix containing the optical power of the M LEDs corresponding to the L reference points in the test set is inputted to the trained BP neural network model. Meanwhile, the input matrix of the neural network test dataset can be expressed as

$$\bar{X}^{\mathrm{T}} = \begin{pmatrix} \bar{X}_1 \\ \bar{X}_2 \\ \vdots \\ \bar{X}_L \end{pmatrix}^{\mathrm{T}} = \begin{pmatrix} P_{11}, P_{12}, \ldots, P_{1M} \\ P_{21}, P_{22}, \ldots, P_M \\ \vdots \\ P_{L1}, P_{L2}, \ldots, P_{LM} \end{pmatrix}^{\mathrm{T}}_{L\times M} \tag{30}$$

$\bar{X}_q = (P_{q1}, P_{q2}, \ldots, P_{qM})$ denotes the light power values of the M LED light sources as received by the q-th reference fingerprint point in the test set. The corresponding output matrix is

$$\overline{Y}^{\mathrm{T}} = \begin{pmatrix} \overline{Y_1} \\ \overline{Y_2} \\ \vdots \\ \overline{Y_L} \end{pmatrix} = \begin{pmatrix} \overline{x_1} & \overline{y_1} & \overline{z_1} \\ \overline{x_2} & \overline{y_2} & \overline{z_1} \\ \vdots & \vdots & \vdots \\ \overline{x_L} & \overline{y_L} & \overline{z_L} \end{pmatrix}^{\mathrm{T}} \tag{31}$$

$\overline{Y_q} = (\overline{x_q}, \overline{y_q}, \overline{z_q})(1 \le q \le L)$ are the predicted coordinates of the q-th reference fingerprint point in the test set.

III. Numerical Simulation and Experimental Verification

1. Numerical simulation

An indoor positioning environment was built, and an experiment was performed in the three-dimensional space model ($L = W = 4$ m, $H = 3$ m). The coordinates of the four LED light sources were L_1 (0.6 m, 0.6 m, 3 m), L_2 (0.6 m, 3.4 m, 3 m), L_3 (3.4 m, 3.4 m, 3 m), and L_4 (3.4 m, 0.6 m, 3 m), respectively. Grid calibration was performed upon the receiving plane using a 5 cm mesh. The four LED light sources were loaded with sinusoidal signals of different frequencies at the transmitting end, and the frequencies and corresponding optical powers of the four LED light sources were separated via the Pisarenko harmonic decomposition algorithm at each fingerprint point of the plane, using the spatial channel simulation parameters shown in Table 1.

Figure 3 shows the signal frequency discrimination and power extraction effects for multiple LED light sources at different detection positions. The results are as follows: when the signal-to-noise ratio is 10 dB, the predicted frequency does not deviate significantly from the power value, and the maximum frequency error is 0.104 Hz;

Table 1 Simulation parameters

Parameter	Value
Model room	4 m × 4 m × 3 m
LED bead power	5 W
LED1 loading frequency LED2 loading frequency LED3 loading frequency LED4 loading frequency	100 Hz 300 Hz 500 Hz 700 Hz
LED bead half-power angle Receiving area of photodetector (A) Focus lens gain (g) Optical filter gain (T_S)	54° 2 cm^2 1.5 1.5
Incident angle of photodetector receiver (φ) Photodetector conversion efficiency (R)	60° 0.4 A/W

the power change is sensitive to the distance of the positioning point, and the maximum error of the power estimation is 0.0362 W; the extracted power value of each LED (as the training input data) has good stability and high recognition.

Figure 4 shows the three-dimensional simulation positioning error maps when $H = 0$ m, 0.5 m, 1.0 m, and 1.5 cm, respectively. The hollow green circle indicates the real position coordinates, and the red star denotes the position coordinates measured by the BP neural network. When $H = 0$ m, 0.5 m, 1.0 m, and 1.5 cm, the average errors are 5.75 cm, 3.56 cm, 2.12 cm, and 1.19 cm, respectively, and the overall three-dimensional positioning average positioning error is 3.18 cm.

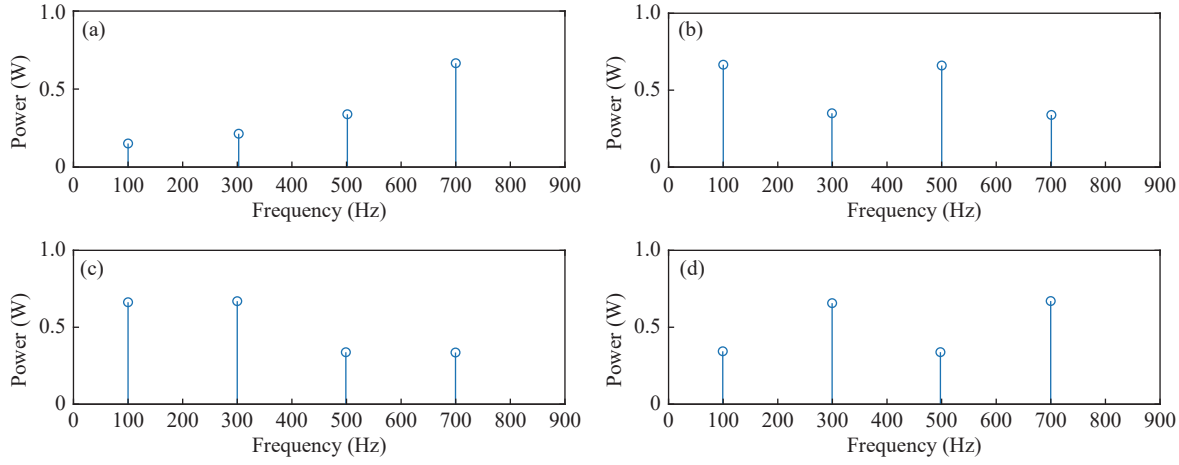

Figure 3 Estimated signal frequency-power distribution at different coordinates. (a) (4, 1, 0); (b) (2, 3, 0); (c) (1, 2, 0); (d) (2, 1, 0).

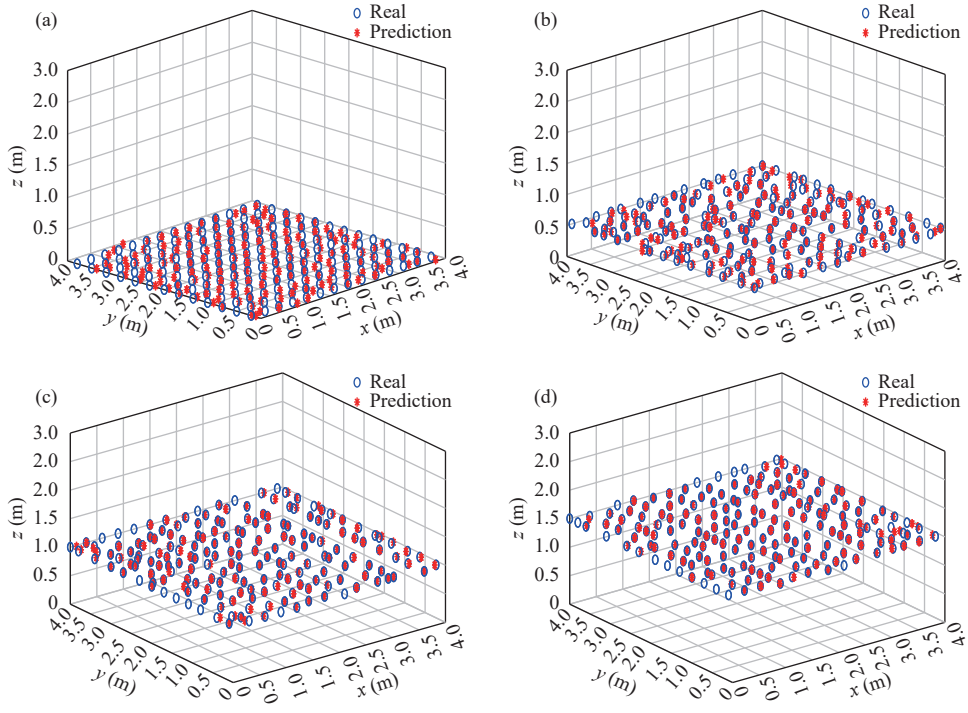

Figure 4 Four-dimensional distribution of positioning errors in different planes for indoor visible light localization. (a) $H = 0$ m; (b) $H = 0.5$ m; (c) $H = 1.0$ m; and (d) $H = 1.5$ m.

2. Experimental verification

We set up a 3D test space with a side length of 0.8 m, as shown in Figure 5. Concerning the positioning system design in the paper, NLT5W is chosen as the LED light source, with rated power of 5 W for each LED lamp. Meanwhile, PIN photodiode of LSSPD-3.5 is chosen as the receiving end detector of the system. We arranged four LED light sources on top of the space and established a two-dimensional coordinate system with the corner of the bottom plane as the origin. In the bottom plane of the space, the grid points were divided at 5 cm intervals, and 289 equally spaced measurement positions were selected. At the transmitter side, the signal generator generated sinusoidal signals of different frequencies and loaded them to the corresponding LED light source via the light drive circuit, such that the LED sent light signals periodically. At the receiving end, the PD was used as a signal receiver; it was placed horizontally at 289 equally spaced measurement positions in the positioning area, to convert the received optical signal into an electrical one. Then, using the Pisarenko harmonic decomposition algorithm, we separated and obtained the light power vectors corresponding to the four LED light sources at the measurement positions. Finally, using the neural network positioning algorithm, 289 sets of training data and 20 sets of test data were selected for multiple tests, to obtain the location coordinates of the PD.

Some of the extracted light power data are shown in Table 2, which shows the light power values and corresponding position coordinates of LED_1, LED_2, LED_3, and LED_4, respectively. Using the proposed neural network positioning algorithm, 289 sets of data were imported into the neural network for processing and training.

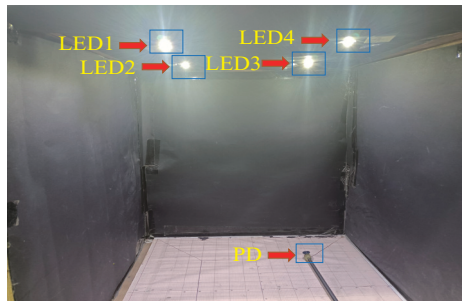

Figure 5 Experimental setup.

After multiple positioning tests on the selected 289 sets of training data and 20 sets of test data, the positioning error distribution diagram shown in Figure 6 was obtained. The results show that the probability of an error of less than 5 cm was 60%, and the probability of an error below 2 cm was 10%; the average positioning error was 4.28 cm, which shows that the proposed algorithm has a high positioning accuracy and stable positioning effect.

IV. Conclusions

The traditional RSS-based visible-light indoor positioning system cannot accurately obtain the attenuation factor for each LED light in space transmission processes. A visible-light indoor location model, based on a combination of the Pisarenko harmonic decomposition algorithm and a BP neural network, was proposed. The algorithm improved the frequency estimation and power extraction capabilities for multiple LED light sources loaded with sinusoidal signals of different frequencies under

Table 2 Actual training data

x	y	LED_1	LED_2	LED_3	LED_4	x	y	LED_1	LED_2	LED_3	LED_4
0	0.00	38.97	19.33	10.01	15.84	0.05	0.00	42.84	20.16	11.61	19.35
0	0.05	41.63	20.70	11.09	17.15	0.05	0.05	45.18	22.79	12.47	19.80
0	0.10	41.49	21.44	11.69	17.28	0.05	0.10	47.16	25.47	13.41	19.80
0	0.15	45.14	26.15	14.06	18.68	0.05	0.15	48.87	28.76	14.69	20.48
0	0.20	45.61	27.90	13.25	17.19	0.05	0.20	49.32	31.37	15.41	20.52
0	0.25	45.18	31.14	13.70	18.25	0.05	0.25	48.51	34.70	16.16	19.98
0	0.30	44.82	35.10	14.99	17.19	0.05	0.30	46.71	38.12	16.90	19.44
0	0.35	42.84	37.85	15.89	16.83	0.05	0.35	44.33	40.86	17.03	18.13
0	0.40	41.13	40.86	17.17	16.81	0.05	0.40	40.73	42.84	16.63	15.91
0	0.45	37.76	42.75	18.47	14.78	0.05	0.45	38.39	45.45	17.44	15.48
0	0.50	34.50	46.62	20.09	14.60	0.05	0.50	35.01	48.60	18.47	14.83
0	0.55	32.00	47.88	21.13	14.29	0.05	0.55	32.40	49.14	18.63	13.91
0	0.60	27.85	46.71	19.67	12.53	0.05	0.60	29.84	50.58	21.44	14.96
0	0.65	24.30	45.45	17.89	11.10	0.05	0.65	27.09	50.2	22.12	14.31
0	0.70	21.15	44.33	17.12	10.66	0.05	0.70	24.03	49.05	20.81	12.78
0	0.75	19.62	43.34	16.79	9.94	0.05	0.75	21.47	47.61	20.39	11.79
0	0.80	18.77	40.77	15.10	8.94	0.05	0.80	19.85	43.97	19.07	11.68

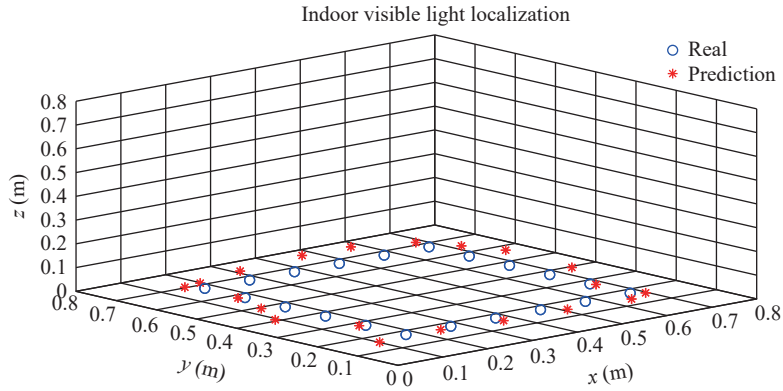

Figure 6 Distribution of measurement positioning errors.

conditions of colored noise and low signal-to-noise ratios (SNRs). The individual power values of each LED light source were trained and tested in the neural network; they significantly improved the indoor positioning accuracy of the visible-light system, to achieve accurate positioning. In the simulation stage, the maximum frequency detection error was 0.104 Hz and the maximum power detection error was 0.0362 W when SNR = 10 dB. The algorithm was applied to a wooden stereo model with a side length of 0.8 m, and 289 groups of training data and 20 groups of test data were randomly selected to perform the actual positioning test. The average error was 4.28 cm, making this a feasible scheme for visible-light indoor positioning technology.

Acknowledgement

This work was supported by the National Defense Foundation of China (Grant No. 61671362), General project of industrial field of Shaanxi science and Technology Department (Grant No. 2022GY-072), Xi'an Science and technology project (Grant No. 2020KJRC0040).

References

[1] Y. Tao and L. Zhao, "A novel system for WiFi radio map automatic adaptation and indoor positioning," *IEEE Transactions on Vehicular Technology*, vol. 67, no. 11, pp. 10683–10692, 2018.

[2] C. C. Yang and H. R. Shao, "WiFi-based indoor positioning," *IEEE Communications Magazine*, vol. 53, no. 3, pp. 150–157, 2015.

[3] T. Komine and M. Nakagawa, "Fundamental analysis for visible-light communication system using LED lights," *IEEE Transactions on Consumer Electronics*, vol. 50, no. 1, pp. 100–107, 2004.

[4] J. B. Fang, Z. Yang, S. Long, *et al.*, "High-speed indoor navigation system based on visible light and mobile phone," *IEEE Photonics Journal*, vol. 9, no. 2, article no. 8200711, 2017.

[5] M. T. Van, N. Van Tuan, T. T. Son, *et al.*, "Weighted *k*-nearest neighbour model for indoor VLC positioning," *IET Communications*, vol. 11, no. 6, pp. 864–871, 2017.

[6] K. Wang, A. Nirmalathas, C. Lim, *et al.*, "Indoor infrared optical wireless localization system with background light power estimation capability," *Optics Express*, vol. 25, no. 19, pp. 22923–22931, 2017.

[7] G. Chen, W. K. Chen, Q. Y. Yang, *et al.*, "A novel visible light positioning system with event-based neuromorphic vision sensor," *IEEE Sensors Journal*, vol. 20, no. 17, pp. 10211–10219, 2020.

[8] I. M. Abou-Shehada, A. F. AlMuallim, A. K. AlFaqeh, *et al.*, "Accurate indoor visible light positioning using a modified pathloss model with sparse fingerprints," *Journal of Lightwave Technology*, vol. 39, no. 20, pp. 6487–6497, 2021.

[9] H. L. Yang, W. D. Zhong, C. Chen, *et al.*, "Coordinated resource allocation-based integrated visible light communication and positioning systems for indoor IoT," *IEEE Transactions on Wireless Communications*, vol. 19, no. 7, pp. 4671–4684, 2020.

[10] S. H. Yang, H. S. Kim, Y. H. Son, *et al.*, "Three-dimensional visible light indoor localization using AOA and RSS with multiple optical receivers," *Journal of Lightwave Technology*, vol. 32, no. 14, pp. 2480–2485, 2014.

[11] N. Knudde, W. Raes, J. De Bruycker, *et al.*, "Data-efficient Gaussian process regression for accurate visible light positioning," *IEEE Communications Letters*, vol. 24, no. 8, pp. 1705–1709, 2020.

[12] S. Y. Jung, S. Hann, and C. S. Park, "TDOA-based optical wireless indoor localization using LED ceiling lamps," *IEEE Transactions on Consumer Electronics*, vol. 57, no. 4, pp. 1592–1597, 2011.

[13] K. Majeed and S. Hranilovic, "Performance bounds on passive indoor positioning using visible light," *Journal of Lightwave Technology*, vol. 38, no. 8, pp. 2190–2200, 2020.

[14] R. Amsters, D. Holm, J. Joly, *et al.*, "Visible light positioning using Bayesian filters," *Journal of Lightwave Technology*, vol. 38, no. 21, pp. 5925–5936, 2020.

[15] L. Zhao, Z. G. Liu, and D. Wang, "Research on multi-point calibration linear approximation indoor positioning algorithm based on LED array," in *Proceedings of 2018 5th International Conference on Systems and Informatics*, Nanjing, China, pp. 751–756, 2018.

[16] W. P. Guan, Y. X. Wu, S. S. Wen, *et al.*, "Indoor positioning technology of visible light communication based on CDMA modulation," *Acta Optica Sinica*, vol. 36, no. 11, article no. 11060061, 2016. (in Chinese)

[17] H. S. Kim, D. R. Kin, S. H. Yang, *et al.*, "An indoor visible light communication positioning system using a RF carrier allocation technique," *Journal of Lightwave Technology*, vol. 31, no. 1, pp. 134–144, 2013.

[18] L. Bai, Y. Yang, C. Y. Feng, *et al.*, "Received signal strength assisted perspective-three-point algorithm for indoor visible light positioning," *Optics Express*, vol. 28, no. 19, pp. 28045–28059, 2020.

[19] X. S. Guo, S. H. Shao, N. Ansari, *et al.*, "Indoor localization using visible light via fusion of multiple classifiers," *IEEE Photonics Journal*, vol. 9, no. 6, pp. 1–16, 2017.

[20] L. Bai, Y. Yang, Z. T. Zhang, *et al.*, "A high-coverage cam-

era assisted received signal strength ratio algorithm for indoor visible light positioning," *IEEE Transactions on Wireless Communications*, vol. 20, no. 9, pp. 5730–5743, 2021.

[21] G. Seco-Granados, J. López-Salcedo, D. Jiménez-Baños, *et al.*, "Challenges in indoor global navigation satellite systems: unveiling its core features in signal processing," *IEEE Signal Processing Magazine*, vol. 29, no. 2, pp. 108–131, 2012.

[22] Y. C. Wu, C. W. Chow, Y. Liu, *et al.*, "Received-signal-strength (RSS) based 3D visible-light-positioning (VLP) system using kernel ridge regression machine learning algorithm with sigmoid function data preprocessing method," *IEEE Access*, vol. 8, pp. 214269–214281, 2020.

[23] W. J. Gu, M. Aminikashani, P. Deng, *et al.*, "Impact of multipath reflections on the performance of indoor visible light positioning systems," *Journal of Lightwave Technology*, vol. 34, no. 10, pp. 2578–2587, 2016.

[24] F. Alam, M. T. Chew, T. Wenge, *et al.*, "An accurate visible light positioning system using regenerated fingerprint database based on calibrated propagation model," *IEEE Transactions on Instrumentation and Measurement*, vol. 68, no. 8, pp. 2714–2723, 2019.

[25] C. W. Chow, Y. Liu, C. H. Yeh, *et al.*, "A practical in-home illumination consideration to reduce data rate fluctuation in visible light communication," *IEEE Wireless Communications*, vol. 22, no. 2, pp. 17–23, 2015.

[26] Z. H. Yang, W. Xu, and Y. R. Li, "Fair non-orthogonal multiple access for visible light communication downlinks," *IEEE Wireless Communications Letters*, vol. 6, no. 1, pp. 66–69, 2017.

[27] A. B. M. M. Rahman, T. Li, and Y. Wang, "Recent advances in indoor localization via visible lights: a survey," *Sensors*, vol. 20, no. 5, article no. 1382, 2020.

[28] H. Burchardt, N. Serafimovski, D. Tsonev, *et al.*, "VLC: Beyond point-to-point communication," *IEEE Communications Magazine*, vol. 52, no. 7, pp. 98–105, 2014.

[29] Y. Yang, Z. M. Zeng, J. L. Cheng, *et al.*, "A relay-assisted OFDM system for VLC uplink transmission," *IEEE Transactions on Communications*, vol. 67, no. 9, pp. 6268–6281, 2019.

[30] W. Xu, J. Wang, H. Shen, *et al.*, "Indoor positioning for multiphotodiode device using visible-light communications," *IEEE Photonics Journal*, vol. 8, no. 1, article no. 7900511, 2016.

[31] H. Q. Zhang, J. H. Cui, L. H. Feng, *et al.*, "High-precision indoor visible light positioning using deep neural network based on the Bayesian Regularization with sparse training point," *IEEE Photonics Journal*, vol. 11, no. 3, article no. 7903310, 2019.

Li ZHAO Professor, Master Supervisor, Xi'an Technology University. Her main research interests include optical channel characteristics, channel coding, modulation technology, signal processing in free space optical communication system; light source layout, modulation technology, indoor positioning in visible light communication system. As the project leader, she has undertaken more than ten scientific research projects in the field of optical communication. As a main participant, she has participated in many scientific research projects. She has obtained three national invention patents, one national utility model patent and two software registration rights. She has published more than 50 papers in the field of optical communication. (Email: pilly_lily@126.com)